Kinetic and thermodynamic analysis of Cu2+-dependent reductive inactivation in direct electron transfer-type bioelectrocatalysis by copper efflux oxidase

Taiki Adachi, Ievgen Mazurenko, Nicolas Mano, Yuki Kitazumi, Kunishige Kataoka, Kenji Kano, Keisei Sowa, Elisabeth Lojou

▶ **To cite this version:**

Taiki Adachi, Ievgen Mazurenko, Nicolas Mano, Yuki Kitazumi, Kunishige Kataoka, et al.. Kinetic and thermodynamic analysis of Cu2+-dependent reductive inactivation in direct electron transfer-type bioelectrocatalysis by copper efflux oxidase. Electrochimica Acta, 2022, 429, pp.140987. 10.1016/j.electacta.2022.140987 . hal-03752803

HAL Id: hal-03752803
https://hal.science/hal-03752803v1

Submitted on 17 Aug 2022

HAL is a multi-disciplinary open access archive for the deposit and dissemination of scientific research documents, whether they are published or not. The documents may come from teaching and research institutions in France or abroad, or from public or private research centers.

L'archive ouverte pluridisciplinaire **HAL**, est destinée au dépôt et à la diffusion de documents scientifiques de niveau recherche, publiés ou non, émanant des établissements d'enseignement et de recherche français ou étrangers, des laboratoires publics ou privés.

Revised Manuscript (Clean Version including Abstract) Click here to view linked References

Kinetic and thermodynamic analysis of Cu^{2+}-dependent reductive inactivation in direct electron transfer-type bioelectrocatalysis by copper efflux oxidase

Taiki Adachi[a,b*], Ievgen Mazurenko[a], Nicolas Mano[c], Yuki Kitazumi[b], Kunishige Kataoka[d], Kenji Kano[e], Keisei Sowa[b], and Elisabeth Lojou[a]

a) *Aix Marseille University, CNRS, BIP, Bioénergétique et Ingénierie des Protéines, 31 chemin Aiguier, 13402 Marseille, France*

b) *Division of Applied Life Sciences, Graduate School of Agriculture, Kyoto University, Sakyo, Kyoto 606-8502, Japan*

c) *Centre de Recherche Paul Pascal (CRPP), UMR 5031, CNRS, University of Bordeaux, 33600 Pessac, France*

d) *Division of Material Sciences, Graduate School of Natural Science and Technology, Kanazawa University, Kakuma, Kanazawa 920-1192, Japan*

e) *Center for Advanced Science and Innovation, Kyoto University, Gokasho, Uji, Kyoto 611-0011, Japan*

*Corresponding author: Mr. Taiki Adachi

E-mail address: adachi.taiki.62s@st.kyoto-u.ac.jp

Keywords:

Multicopper oxidase

Copper efflux oxidase

Direct electron transfer

Bioelectrochemistry

Cu^{2+} effects

Abstract

Copper efflux oxidases (CueOs) are key enzymes in copper homeostasis systems. The mechanisms involved are however largely unknown. CueO-type enzymes share a typical structural feature composed of Methionine-rich (Met-rich) domains that are proposed to be involved in copper homeostasis. Bioelectrocatalysis using CueO-type enzymes in the presence of Cu^{2+} recently highlighted a new Cu^{2+}-dependent catalytic pathway related to a cuprous oxidase activity. In this work, we further investigated the effects of Cu^{2+} on direct electron transfer (DET)-type bioelectrocatalytic reduction of O_2 by CueO at NH_2-functionalized multi-walled carbon nanotubes. The DET-type bioelectrocatalytic activity of CueO decreased at low potential in the presence of Cu^{2+}, showing unique peak-shaped voltammograms that we attribute to inactivation and reactivation processes. Chronoamperometry was used to kinetically analyze these processes, and the results suggested linear free energy relationships between the inactivation/reactivation rate constant and the electrode potential. Pseudo-steady-state analysis also indicated that Cu^{2+} uncompetitively inhibited the enzymatic activity. A detailed model for the Cu^{2+}-dependent reductive inactivation of CueO was proposed to explain the electrochemical data, and the related thermodynamic and kinetic parameters. A CueO variant with truncated copper-binding α helices and bilirubin oxidase free of Met-rich domains also showed such reductive inactivation process, which suggests that multicopper oxidases contain copper-binding sites that lead to inactivation.

1. Introduction

Multicopper oxidases (MCOs) are essential enzymes in many organisms and have been widely studied in the biochemistry, electrochemistry, and spectroscopy fields [1,2]. In solution, substrates such as phenols, bilirubin, and ascorbate are oxidized at type I (T1) Cu, and the extracted electrons are transferred to the trinuclear copper cluster (TNC) composed of one type II (T2) Cu and two type III (T3) Cu moieties, where dioxygen (O_2) is reduced into water [1,2]. MCOs are often utilized as O_2-reducing cathodic catalysts for bioelectrochemical applications, such as O_2 biosensors and biofuel cells [3,4]. They can undergo enzymatic reactions on electrode materials that act as electron donors and react with the T1 Cu. Such direct electrical communication between an enzyme and an electrode is called direct electron transfer (DET)-type bioelectrocatalysis [5–9]. For such purposes, carbon nanotube (CNT) networks are widely used as efficient platforms for DET-type bioelectrocatalysis of various enzymes including MCOs [10–13].

Copper efflux oxidase (CueO) belongs to the MCO family. It is supposed to be able to protect periplasmic enzymes from copper mediated toxicity by oxidizing the harmful cuprous ion (Cu^+) [14–17]. Consequently, CueO is proposed to play an important role as a radical scavenger in bacterial copper homeostasis, although the exact mechanism is largely unknown. *Escherichia coli* (*E. coli*) CueO has been the most studied among CueO-type enzymes. Unlike other MCOs such as laccase (Lac) or bilirubin oxidase (BOD), the uniqueness of the E. coli CueO structure is associated with a large segment composed of α helices (helices 5, 6, and 7 from the N-terminus) that cover the T1 Cu site, which results in low catalytic activity toward the oxidation of large electron-donating substrates such as 2,2′-azinobis(3-ethylbenzothiazoline-6-sulfonic acid) (ABTS) [18,19].

In contrast, the helical region provides additional copper-binding sites; consequently, ABTS-oxidizing activity is improved in the presence of excess cupric ion (Cu^{2+}), because the bound coppers mediate the electron transfer between ABTS and the T1 Cu [18–20]. In bioelectrocatalysis, on the other hand, *E. col*i CueO exhibits strong DET-type activity on positively charged electrodes because the surface charge near the T1 Cu site is negative [21]. Hence, positively charged platforms can electrostatically control the enzyme orientation in a manner favorable for the interfacial electron transfer from the electrode to the T1 Cu [21].

Our group recently studied the bioelectrocatalytic reduction of O_2 by Lac from *Thermus thermophilus* (*Tt*Lac). *Tt*Lac structure shows a copper-binding Met-rich hairpin domain near the T1 Cu, thus presenting similarity with *E. coli* CueO [22]. As with *E. coli* CueO, modification of electrodes by positively charged CNTs were found to be favorable for DET, while negative ones prevented DET process. For the first time, it was however demonstrated that addition of Cu^{2+} allowed bioelectrocatalytic O_2 reduction at negative CNTs, at a potential lower than the expected potential for a catalytic process passing through the T1 Cu, hence suggesting a change in the electron transfer pathway between the enzyme and the electrode. The process was tentatively attributed to the cuprous oxidase activity of the enzyme induced by Cu binding to the Met-rich domain. On positively charged CNTs where DET was favored, Cu^{2+} addition induced progressive DET current decrease with simultaneous occurrence of the Cu^{2+}-related catalytic wave. Whatever positive or negative CNTs-based electrodes, voltammograms recorded in the presence of Cu^{2+} were peak-shaped. While the cause of this observation remained unknown, it was suggested that Cu^{2+}-related electrocatalytic activation may be accompanied by an inactivation process. MCO inhibition by H_2O_2 and halides have been

reported [23–28]. As far as we know, MCO inactivation by Cu^{2+} was never reported.

In this study, with the final objective of improving the understanding of copper homeostasis, we examined how Cu^{2+} affects the bioelectrocatalytic properties of CueO, with a special focus on the inactivation caused by Cu^{2+}. We especially analyzed kinetic data in order to discuss a potential inhibition mechanism. In addition, we investigated how the helical structure affects the bioelectrocatalytic properties of wild-type CueO by comparing it with its variant lacking Met-rich α helices and another MCO lacking any Met-rich domains.

2. Experimental

2.1. Materials and chemicals

Recombinant wild-type CueO (rCueO) and its variant truncating α helices 5 to 7 (ΔαCueO) were expressed in *E. coli* and purified according to the literature procedure [18]. BOD from *Bacillus pumilus* (*Bp*BOD) was purified according to the literature procedure [29]. Multi-walled CNTs (MWCNTs) functionalized with -NH_2 groups (CNT-NH_2; diameter: 10 nm, length: 1.5 μm) and -COOH groups (CNT-COOH; diameter: 15 nm, length 5–20 nm) were obtained from Metrohm Dropsens (Spain) and NanoLab Inc. (USA), respectively. MWCNTs without any functionalization (nCNT; diameter: 9.5 nm, length: 1.5 μm) were obtained from Nanocyl SA (Belgium). All other reagents were purchased from Sigma–Aldrich (Merck, Germany). All solutions were prepared using ultrapure water.

2.2. Electrode preparation

Planar glassy carbon electrodes (GCs; diameter: 3 mm) were polished with an alumina slurry, sonicated and washed with distilled water. Then, CNT-NH_2 or nCNT slurry dispersed in *N*-methyl-2-pyrrolidone was applied onto the surface of GCs and dried under reduced pressure. The amount of deposited CNT-NH_2 and nCNT was set to 0.5 μg and 5 μg, respectively. These electrodes are referred to as CNT-NH_2/GCs and nCNT/GCs, respectively. On the other hand, a CNT-COOH slurry dispersed in water was applied onto the surface of GCs and dried under reduced pressure. The amount of deposited CNT-COOH was set to 5 μg. These electrodes are referred to as CNT-COOH/GCs. A 5-μL aliquot of a 20 μM enzyme solution dissolved in 0.1 M phosphate buffer (pH 7.0) was then applied to CNT-NH_2/GC, nCNT/GC, and CNT-COOH/GC, after which the electrodes were placed in a water-saturated atmosphere for 2 h at 4 °C. The enzyme-modified electrodes were washed with buffer solution before electrochemical measurements.

2.3. Electrochemical measurements

All electrochemical measurements were performed at 25 °C using a potentiostat (PGSTAT302N) and a rotating electrode instrument (RRDE) controlled by Nova 2.0 software (Metrohm Autolab, Switzerland). The rotation speed (ω) of the working electrode was set to 4000 rpm. Platinum wire and a Hg|Hg_2SO_4|sat. K_2SO_4 electrode were used as counter and reference electrodes, respectively. In this study, all potentials were converted into potentials against the standard hydrogen electrode (SHE) by adding 0.64 V to the measured potential. 0.1 M acetate buffer at pH 5.0 was used as the electrolyte solution. The atmosphere was controlled by continuously bubbling either O_2 or N_2 gas into the buffer.

2.4. Circular dichroism (CD) spectroscopy

20 μM of proteins in 10 mM acetate buffer (pH 6.0) were analyzed by far-UV CD spectroscopy using a J-715 spectropolarimeter (Jasco, Japan) at 25 °C in a cell with a 0.5-mm path-length. Spectra from an average of 10 accumulated scans were acquired.

3. Results and discussion

3.1. Effects of Cu^{2+} on DET-type O_2 reduction by CueO

Cyclic voltammograms (CVs) recorded for the enzyme-modified CNT-NH_2/GCs are shown in Fig. 1. Clear reversible and sigmoidal waves ascribed to DET-type O_2 reduction catalyzed by rCueO and ΔαCueO were observed in an O_2-saturated atmosphere (broken lines in Figs. 1A and B, respectively). $CuSO_4$ was then added to the buffer solution. As the $CuSO_4$ concentration increased, and as the overpotential increased, the catalytic current density clearly decreased at both the rCueO- and ΔαCueO-modified electrodes, with the occurrence of peak shaped curves (solid lines in Figs. 1A and B, respectively). The irreversibility observed between the forward and reversed scans in each voltammogram also reveals that Cu^{2+} induces kinetic hysteresis in the DET-type O_2 reduction by CueO, which indicates that the Cu^{2+}-dependent process is more slowly than the change in the electrode potential. CVs were recorded at various scan rates (Fig. 2). As the scan rate slowed down, the peak shape was more and more evident. Similar changes in the shapes of the CVs were observed in a study relative to the oxidative inactivation in DET-type bioelectrocatalysis of the O_2-tolerant [NiFe]-hydrogenase [30,31]. By homology, we will refer to "reductive inactivation" to reflect the effects of Cu^{2+} on CueO bioelectrocatalysis.

We previously reported similar abovementioned CV shapes in the case of O_2 reduction by *Tt*Lac immobilized on the same CNT-NH_2 [22]. It could thus be hypothesized that such Cu^{2+}-dependent inactivation is specific to CueO-like enzymes presenting Met-rich domains covering the T1 Cu. However, the inactivation process was also observed using *Bp*BOD, another MCO lacking such domains (Fig. S1). Structural alignments of CueO, *Bp*BOD, and *Tt*Lac proved their high homology (Figs. S2 and S3). While the structure of the three cupredoxin domains and general fold might be the same, the additional Met-rich domain is missing in *Bp*BOD. Thus, we concluded that the Cu^{2+}-dependent inactivation is not related to the Met-rich domain.

The addition of other divalent metal cations (Ca^{2+} and Ni^{2+}) did not result in such a decrease in current (Fig. S4), from which we can conclude that the Cu^{2+}-dependent inactivation in CueO bioelectrocatalysis is not due to any electrostatic interactions caused by additional ions. In addition, the rCueO-modified nCNT/GC also showed similar behavior to the rCueO-modified CNT-NH_2/GC for Cu^{2+} (Fig. S5), which suggests that NH_2 functional groups at MWCNTs are not involved in the Cu^{2+}-dependent inactivation process.

In addition, the involvement of MCOs potentially depleted of the T2 Cu can be ruled out [32–35]. Indeed, since only the catalytic current produced by active enzymes was measured, the presence or absence of the fraction without the T2 Cu do not interfere with the analysis. Furthermore, both DET-type and ABTS-oxidizing activities of CueO were stable for a long while, suggesting that the T2 Cu was maintained in the enzyme and its mobility can be negligible.

Cu^{2+} is electrochemically active on a carbon electrode. The formal potentials of the Cu^{2+}/Cu^0 and Cu^{2+}/Cu^+ redox couples are 0.340 V and 0.159 V, respectively [36],

without consideration of complexation with other ions (acetate in this case). Hence, direct electrochemical reactions involving Cu species may interfere with reductive inactivation of CueO. 1-Electron reduction from Cu^{2+} to Cu^{+} appears to be negligible since the reaction is thermodynamically unfavorable under normal conditions due to the instability of Cu^{+} devoid of desirable ligands in aqueous solution. We recorded multi-scanned CVs swept down to two different cathodic potentials, namely 0.3 V and 0.2 V. Cu^{2+}-dependent reductive inactivation was observed to be reversible during three cycles when the lowest potential was set to 0.3 V (Fig. 3A). In this potential range, redox currents relative to Cu^{2+} were hardly distinguishable from the background (dotted red lines in Fig. 3A). At the abiotic CNT-NH_2/GC in the presence of 1 mM $CuSO_4$, Cu^{2+} reduction to Cu^{0} starts to be involved at lower potentials than 0.3 V, as denoted by the anodic redissolution peak clearly seen in Fig. S6. These results suggest that the reductive inactivation of CueO is not ascribed to direct Cu^{2+} reduction at the electrode, but to some interaction between the enzyme and Cu^{2+} inducing catalysis. In contrast, current density was observed to irreversibly decrease with continuous scanning when the lowest potential was set to 0.2 V (Fig. 3B). Considering that the background cathodic current appeared from 0.3 V (dotted red lines in Fig. 3B), the irreversible decrease in current observed during continuous scanning may be due to the electrodeposition of Cu metal at the electrode surface, which may interfere with the enzyme–electrode interface.

As mentioned in the introduction, Cu^{2+} reportedly enhances rCueO activity for ABTS oxidation in solution most probably through coordination near helices 5–7 [19]. Such enhancement was also observed in DET-type reactions at negatively charged CNTs (CNT-COOH) for rCueO (Fig. S7), in a similar manner to that described previously for *Tt*Lac. It was ascribed to an electron transfer pathway from the additional copper-binding

site to the T1 Cu. However, such enhancement was not observed for both the rCueO- and ΔαCueO-modified CNT-NH_2/GCs, most likely because the enzyme is favorably oriented to promote DET between the T1 Cu and the electrode. In agreement with this assumption, Cu^{2+}-related waves progressively occurred at the CNT-NH_2-based electrode for *Tt*Lac which showed a lower DET-type current than rCueO [22].

On the other hand, Cu^{2+}-dependent reductive inactivation was not observed in the solution reaction, as the addition of Cu^{2+} reportedly enhances CueO activity [18]. The difference in CueO behavior between DET-type bioelectrocatalysis and the solution reaction can be explained from thermodynamic viewpoints. The formal potentials of the electron donors used for assaying CueO activities (e.g., the formal potential of $ABTS^{1-/2-}$ is 0.63 V at pH 5.3 [37]) appear to be too positive to observe Cu^{2+}-dependent reductive inactivation, which was clearly observed at potentials below approximately 0.4 V. This assumption is also in agreement with our previous observation that a mutant of *Tt*Lac with a 100 mV higher potential was indeed inactivated by the addition of Cu^{2+} in solution [38].

3.2. Kinetic analysis of Cu^{2+}-dependent reductive inactivation

In this section, we analyze the kinetics of Cu^{2+}-dependent reductive inactivation of DET-type bioelectrocatalysis by CueOs according to previous reports on [NiFe]-hydrogenase [30,31,39]. First, reversible (bi-directional) inactivation and reactivation are simply expressed by pseudo-first-order reversible kinetics, as follows:

$$\mathrm{E_A} \underset{k_\mathrm{A}}{\overset{k_\mathrm{I}}{\rightleftarrows}} \mathrm{E_I} \qquad (1)$$

where E_A and E_I are enzymes in the active and inactive states, respectively, and k_I and k_A

are the apparent reaction kinetic constants for inactivation and reactivation, respectively. This kinetic equation can be solved for the surface concentration of E_A (= $[E_A]$), and the catalytic current density (j_{cat}) linearly depends on $[E_A]$. Thus, j_{cat} is expressed as follows [31]:

$$j_{\mathrm{cat}} = j_0 \left\{ \frac{k_\mathrm{I}}{k_\mathrm{I} + k_\mathrm{A}} \exp[-(k_\mathrm{I} + k_\mathrm{A})t] + \frac{k_\mathrm{A}}{k_\mathrm{I} + k_\mathrm{A}} \right\} \quad (2)$$

where t is time and j_0 is j_{cat} at $t = 0$.

On the other hand, the apparent limiting current density (j_{app}) at a rotating disk electrode is expressed by Koutecký–Levich equation:

$$\frac{1}{j_{\mathrm{app}}} = \frac{1}{j_{\mathrm{mt}}} + \frac{1}{j_{\mathrm{cat}}} \quad (3)$$

where j_{mt} is the current density controlled by the mass transfer of the substrate (O_2), and is expressed by Levich equation:

$$j_{\mathrm{mt}} = -0.62 n_{\mathrm{O_2}} F D_{\mathrm{O_2}}^{\frac{2}{3}} \nu^{-\frac{1}{6}} c_{\mathrm{O_2}} \omega^{\frac{1}{2}} \quad (4)$$

where n_{O_2}, F, D_{O_2}, ν, and c_{O_2} are the number of electrons of O_2 reduction (= 4), the Faraday constant, the diffusion constant of O_2 (= 2.0×10^{-5} cm^2 s^{-1} at 25 °C [40]), the kinematic viscosity of the buffer (= 0.009 cm^2 s^{-1} at 25 °C [41]), and the bulk concentration of O_2 (= 1.2 mM at 25 °C under O_2-saturated conditions [42]), respectively. Thus, j_{mt} is calculated to be –9.5 mA cm^{-2} under O_2-saturated conditions at ω = 4000 rpm.

In the following analysis, we considered the contribution of j_{mt} and converted the experimentally measured j_{app} into j_{cat} by Eq. (3). Using k_I and k_A as adjustable parameters, Eq. (2) was fitted to chronoamperograms (CAs) by non-linear regression analysis using Gnuplot®. To simplify the model, j_0 was considered to be equal to the value of j_{cat} measured in each CA prior to the addition of $CuSO_4$. To neglect interference of the charging current, experimental data acquired in the 0–1 s range were removed prior to

analysis. All CAs were recorded after the working electrode was set to 0.8 V for 30 s to completely reactivate enzymes. The fitted results are shown in Figs. 4 and S8, and the refined values of k_I and k_A are shown in Figs. S9 and S10. The collected data are summarized in Fig. 5 to facilitate a simple comparison of rCueO and ΔαCueO.

Linear free energy relationships between the potential and the common logarithms of k_I and k_A were observed to some extent (Figs. 5A and 5B), which suggests that k_I and k_A partly obey the Butler–Volmer equation. Partial non-linearity especially shown in log (k_I / s^{-1}) vs. E plots is probably due to the small contribution of the Butler–Volmer equation in the analyzed potential range. In contrast, k_I clearly showed a proportional relationship with the Cu^{2+} concentration (Fig. 5C), whereas k_A is less dependent on the Cu^{2+} concentration (Fig. 5D). These results indicate that inactivation and activation are induced by the coordination and dissociation processes of a single Cu^{2+} ion, respectively, and that k_I is more contributed by the Cu^{2+} coordination than the Butler–Volmer equation in this range of the potential and the Cu^{2+} concentration. However, these relationships were not observed under all measurement conditions (Figs. S9 and S10); hence, the reductive inactivation of CueO cannot be completely explained using the simplest model (Eq. (1)). In addition, we could not find clear differences between rCueO and ΔαCueO from the kinetic viewpoints.

3.3. Discussion on inhibition mechanism

We investigated the inhibition mechanism of CueO by Cu^{2+}. It is well-known that inhibition mechanisms of enzymes can be estimated from steady-state reaction kinetics at variable concentrations of substrate and inhibitor. Accordingly, we recorded CAs at the rCueO- and ΔαCueO-modified CNT-NH_2/GCs at different O_2 and Cu^{2+}

concentrations (c_{O2} and c_{Cu}^{2+}, respectively), and calculated j_{cat} by considering various j_{mt} values. We subsequently assumed that steady-state conditions were achieved at t = 30 s; hence, we plotted j_{cat}^{-1} values at t = 30 s as functions of c_{O2}^{-1} and c_{Cu}^{2+}, respectively (Figs. 6, S11, and S12). j_{cat}^{-1} values calculated under low O_2 concentrations included large errors, which are probably due to the large contribution of the mass transfer of O_2 that provides mathematical errors for Koutecký–Levich equation. Both Lineweaver–Burk and Dixon plots partly showed some parallelism, which suggests uncompetitive inhibition in which the inhibitor binds to the enzyme–substrate (ES) complex [43,44]. In contrast, parallelism was not clearly observed at E = 0.3 V in the presence of 0.5 mM or higher Cu^{2+} (Figs. S11A, S11B, S12A, and S12B), which is plausibly due to irreversible enzyme denaturation by the electrodeposition of Cu metal at low potentials.

Based on previous discussion and results of the kinetic analysis, the characteristics of the Cu^{2+}-dependent reversible reductive inactivation and oxidative reactivation in CueO bioelectrocatalysis are summarized as follows: 1) both rates of inactivation and reactivation are exponentially related to the electrode potential, 2) the rate of inactivation is linearly related to c_{Cu}^{2+}, 3) the rate of reactivation is independent of c_{Cu}^{2+}, and 4) Cu^{2+} binds the ES complex. Accordingly, we propose the detailed model shown in Scheme 1 for the Cu^{2+}-dependent reversible reductive inactivation and oxidative reactivation observed in CueO bioelectrocatalysis.

Here, we assume that the inactivation/reactivation cycle can be divided into non-electrochemical and electrochemical processes; the former corresponds to coordination/dissociation between the ES complex and Cu^{2+}, while the latter corresponds to reduction/oxidation of the ES-Cu^{2+} complex. In addition, the complex of ES and $Cu^{2+/1+}$ was assumed to have an active oxidized state (ES-Cu^{2+}) and an inactive reduced state

(ES-Cu^{+}). In this model, the steady-state catalytic current density ($j_{cat,s}$) can be derived from the calculation written in the Appendix A, and the final equation is expressed as:

$$j_{cat,s} = \frac{j_{max}}{1 + \frac{\eta_1^{0.5}}{\frac{k^\circ{}_1}{k_c}} + \frac{\frac{K_{O_2}}{c_{O_2}}(1+\eta_1) + \frac{c_{Cu^{2+}}}{K_{Cu^{2+}}}\eta_2^{-1}}{1 + \frac{c_{Cu^{2+}}}{K_{Cu^{2+}}}}} \quad (5)$$

where j_{max}, $k^\circ{}_1$, k_c, K_{O2} and $K_{Cu}{}^{2+}$ are the maximum catalytic current density, the standard rate constant for the heterogeneous electron transfer between the electrode and the T1 Cu center of CueO, the catalytic constant, and the Michaelis constants of the enzyme for O_2 and Cu^{2+}, respectively. To simplify the analysis, the transfer coefficient is assumed to be 0.5 and η_n is expressed as:

$$\eta_n = \exp\left\{\frac{F}{RT}(E - E^{\circ\prime}{}_n)\right\} \quad (n = 1,2) \quad (6)$$

where $E^{\circ\prime}{}_1$ and $E^{\circ\prime}{}_2$ are the formal potentials of the T1 Cu center and the Cu^{2+}-binding site of CueO, respectively, F is the Faraday constant, R is the gas constant, and T is the absolute temperature. The number of electrons in the rate-determining step involved in the heterogeneous electron transfer was set to 1. The standard rate constant for the heterogeneous electron transfer between the electrode and the Cu^{2+}-binding site of CueO (= $k^\circ{}_2$) was also defined; however, $j_{cat,s}$ is independent of $k^\circ{}_2$. The literature values of K_{O2} are 0.017 mM for rCueO and 0.012 mM for ΔαCueO, respectively [45], which are much smaller than c_{O2} (= 1.2 mM) under O_2-saturated conditions. Hence, Eq. (5) can be simplified, as follows:

$$j_{cat,s} = \frac{j_{max}}{1 + \frac{\eta_1^{0.5}}{\frac{k^\circ{}_1}{k_c}} + \frac{\frac{c_{Cu^{2+}}}{K_{Cu^{2+}}}\eta_2^{-1}}{1 + \frac{c_{Cu^{2+}}}{K_{Cu^{2+}}}}} \quad (7)$$

To consider the enzyme orientation, then, we distributed three k°_1 values: k°_{max} (maximum k°), $k^{\circ}_{max}/10$, and $k^{\circ}_{max}/10^2$. Moreover, the proportion of k°_1 was set to p_1, p_2, and p_3 (= 1 – p_1 – p_2), which correspond to k°_{max}, $k^{\circ}_{max}/10$, and $k^{\circ}_{max}/10^2$, respectively. Thus, Eq. (7) can be rewritten as follows:

$$j_{\mathrm{cat,s}} = \sum_{n=1}^{3} p_n \frac{j_{\max}}{1 + \dfrac{\eta_1^{0.5}}{\dfrac{k^{\circ}_{\max}}{k_{\mathrm{c}}} \times 10^{-(n-1)}} + \dfrac{\dfrac{c_{\mathrm{Cu^{2+}}}}{K_{\mathrm{Cu^{2+}}}} \eta_2^{-1}}{1 + \dfrac{c_{\mathrm{Cu^{2+}}}}{K_{\mathrm{Cu^{2+}}}}}} \tag{8}$$

We determined values for the kinetic and thermodynamic parameters using Eq. (8). Firstly, the voltammograms in the absence of Cu^{2+} under O_2-saturated conditions were fitted to Eq. (8) (Figs. 1A and 1B) using Gnuplot®, in order to refine $E^{\circ\prime}_1$, k°_{max}/k_c, j_{max}, p_1, p_2, and p_3. The refined data are summarized in Table 1 and the fitted results are shown in Fig. 7. The values of $E^{\circ\prime}_1$ and $-j_{max}$ are almost identical for rCueO and ΔαCueO, while ΔαCueO exhibited a larger k°_{max}/k_c value than rCueO, which indicates that ΔαCueO is oriented more favorably for DET on the CNT-NH_2/GC. These results are mostly consistent with those of our previous study in which we investigated DET-type bioelectrocatalysis by CueO at amine-functionalized Ketjen Black-modified electrodes [21].

We also attempted to refine $E^{\circ\prime}_2$ and $K_{Cu}{}^{2+}$ using other fixed parameters ($E^{\circ\prime}_1$, k°_{max}/k_c, p_1, p_2, and p_3) and j_{cat} values at t = 30 s recorded at E = 0.45, 0.40, 0.35, and 0.30 V under O_2-saturated conditions in the presence of Cu^{2+}. Here, j_{max} was set as to be flexible to account for sample variability. Unfortunately, $E^{\circ\prime}_2$ and $K_{Cu}{}^{2+}$ were unable to be determined owing to parameter flexibility, large j_{cat} errors, and the narrow potential range.

Considering the existence of the unidentified Cu^{2+}-binding site in the crystal structure of rCueO elucidated in the presence of 25 mM Cu^{2+} [16], $K_{Cu}{}^{2+}$ seems much larger than 1 mM. The CD spectra also suggest that the secondary structure of CueO is almost conserved in the presence of 1 mM Cu^{2+} (Fig. S13), consistent with a large $K_{Cu}{}^{2+}$ value for CueO. Eq. (8) can be simplified to Eq. (9) when we assume that $c_{Cu}{}^{2+} << K_{Cu}{}^{2+}$:

$$j_{\mathrm{cat,s}} = \sum_{n=1}^{3} p_n \frac{j_{\max}}{1 + \dfrac{\eta_1^{0.5}}{\dfrac{k^{\circ}{}_{\max}}{k_{\mathrm{c}}} \times 10^{-(n-1)}} + \dfrac{c_{\mathrm{Cu}^{2+}} \exp\left(-\dfrac{FE}{RT}\right)}{K_{\mathrm{Cu}^{2+}} \exp\left(-\dfrac{FE^{\circ\prime}{}_2}{RT}\right)}} \tag{9}$$

Using Eq. (9), $j_{\max}$ and $K_{\mathrm{Cu}^{2+}} \exp\left(-\frac{FE^{\circ\prime}{}_2}{RT}\right)$ were refined by Gnuplot®. The refined parameters are listed in Table 2. Theoretical steady-state voltammograms for Cu^{2+}-dependent reductive inactivation are shown in Fig. 8. While the refined curves successfully reproduce the E- and $c_{Cu}{}^{2+}$-dependent current decreases, the actual $K_{Cu}{}^{2+}$ and $E^{\circ\prime}{}_2$ values was difficult to determine because of their strong statistical correlation. On the other hand, there seems no significant differences in the values of $K_{\mathrm{Cu}^{2+}} \exp\left(-\frac{FE^{\circ\prime}{}_2}{RT}\right)$ between rCueO and ΔαCueO, which is consistent with the hypothesis that Cu^{2+} does not coordinate close to the helical regions but near the TNC and T1 Cu centers.

The conformations of the TNC and T1 Cu centers in the ES complex dynamically change during the catalytic cycle [46,47]. Focusing on the mechanism of uncompetitive inhibition, we suggest that the Cu^{2+}-binding site is located near the TNC and the T1 Cu centers because only the ES complex appears to be sensitive to Cu^{2+}. Three His residues that are generally known to be ligands for $Cu^{2+/1+}$ and other metal cations are present within 16 Å of the TNC center, except for its ligands (His145, His488, and His494 shown in Fig. 9). Consequently, we suggest that Cu^{2+} coordinated to some His residues is

electrochemically reduced and induces conformational changes near the TNC center, which inhibits the dynamic transitions of the TNC and T1 Cu centers. In particular, the crystal structure of rCueO in the presence of 10 mM $CuCl_2$ shows that His145 is coordinated to an additional Cu (referred to as Cu6) [48]. Furthermore, His145 is close to His143 and Glu506; the former is a ligand for one of the T3 Cu pair, while the latter is suggested to play an important role in the proton relay of the intermediates during the catalytic cycle [43]. Hence, we concluded that His145 is the most likely to be a ligand for Cu^{2+} which induced the reductive inactivation. The proposed mechanism for the Cu^{2+}-dependent reductive inactivation of CueO is shown in Scheme 2. More information is expected to be obtained by investigating the effects of Cu^{2+} on other DET-type enzymes.

4. Conclusions

We kinetically and thermodynamically analyzed the Cu^{2+}-dependent reductive inactivation of the DET-type bioelectrocatalytic activities of rCueO and ΔαCueO at NH_2-functionalized MWCNTs. Linear free energy relationships seem to exist between the inactivation/reactivation rate constants and the electrode potential, and uncompetitive inhibition mechanism appears to operate. We constructed a detailed model for reversible inactivation and reactivation, and determined thermodynamic data. Further spectroscopic analyses may identify the precise inhibition mechanism. Comparison of crystal structures suggest that this Cu^{2+}-inactivation process is not exclusively encountered in CueO-like proteins, i.e. those enzymes presenting Met-rich domains covering the T1 Cu. This suggests that MCOs contain additional copper-binding sites other than the T1 Cu and TNC, which can be responsible for catalytic inhibition. Using various techniques in spectroscopy, eventually coupled to electrochemistry, biochemistry,

structural biology and theoretical chemistry, a detailed inhibition mechanism focusing on intermediates during the catalytic cycle may be elucidated. By combining in vitro studies of the effects of $Cu^{2+/1+}$ on MCO-based electrocatalysis and in vivo copper resistance, an improved understanding of copper homeostasis in microorganisms is expected. In fine, this study can be extended to other copper-efflux enzymes and will lead to the elucidation of molecular factors involved in copper homeostasis.

Acknowledgements

This work was supported by the sponsorship of JSPS Overseas Challenge Program for Young Researchers (to T.A.) and by National Research Agency (ANR, France) (N°ANR-21-CE44-0024), CNRS, France. We would like to thank Editage (www.editage.com) for English language editing.

Appendix A. Solution for Eq. (5)

Based on the model shown in Scheme 1, the differential equations for the surface concentrations of all states of the enzyme ($[E_R]$, $[E_O]$, [ES], $[ES\text{-}Cu^{2+}]$, and $[ES\text{-}Cu^{+}]$) are expressed as follows:

$$\frac{d[\mathrm{E_R}]}{dt} = -(k_1 + k_{\mathrm{b1}})[\mathrm{E_R}] + k_{\mathrm{f1}}[\mathrm{E_O}] + k_{-1}[\mathrm{ES}] \quad (\mathrm{A.1})$$

$$\frac{d[\mathrm{E_O}]}{dt} = k_{\mathrm{b1}}[\mathrm{E_R}] - k_{\mathrm{f1}}[\mathrm{E_O}] + k_{\mathrm{c}}[\mathrm{ES}] + k_{\mathrm{c}}[\mathrm{ES\text{-}Cu^{2+}}] \quad (\mathrm{A.2})$$

$$\frac{d[\mathrm{ES}]}{dt} = k_1[\mathrm{E_R}] - (k_{-1} + k_{\mathrm{c}} + k_2)[\mathrm{ES}] + k_{-2}[\mathrm{ES\text{-}Cu^{2+}}] \quad (\mathrm{A.3})$$

$$\frac{d[\mathrm{ES\text{-}Cu^{2+}}]}{dt} = k_2[\mathrm{ES}] - (k_{\mathrm{c}} + k_{-2} + k_{\mathrm{f2}})[\mathrm{ES\text{-}Cu^{2+}}] + k_{\mathrm{b2}}[\mathrm{ES\text{-}Cu^{+}}] \quad (\mathrm{A.4})$$

$$\frac{d[\mathrm{ES\text{-}Cu^{+}}]}{dt} = k_{\mathrm{f2}}[\mathrm{ES\text{-}Cu^{2+}}] - k_{\mathrm{b2}}[\mathrm{ES\text{-}Cu^{+}}] \quad (\mathrm{A.5})$$

The surface concentration of the total enzyme ($[E_{total}]$) is defined as:

$$[E_{total}] = [E_R] + [E_O] + [ES] + [ES\text{–}Cu^{2+}] + [ES\text{–}Cu^{+}] \quad (A.6)$$

Under steady-state conditions:

$$\frac{d[E_R]}{dt} = \frac{d[E_O]}{dt} = \frac{d[ES]}{dt} = \frac{d[ES\text{–}Cu^{2+}]}{dt} = \frac{d[ES\text{–}Cu^{+}]}{dt} = 0 \quad (A.7)$$

Using (A.1) to (A.7):

$$[ES\text{–}Cu^{+}] = \frac{k_{f2}}{k_{b2}}[ES\text{–}Cu^{2+}] \quad (A.8)$$

$$[ES] = \left(\frac{k_c}{k_2} + \frac{k_{-2}}{k_2}\right)[ES\text{–}Cu^{2+}] \quad (A.9)$$

$$[E_R] = \left[\left(\frac{k_{-1}}{k_1} + \frac{k_c}{k_1}\right)\left(\frac{k_c}{k_2} + \frac{k_{-2}}{k_2}\right) + \frac{k_c}{k_1}\right][ES\text{–}Cu^{2+}] \quad (A.10)$$

$$[E_O] = \left\{\frac{k_{b1}}{k_{f1}}\left[\left(\frac{k_{-1}}{k_1} + \frac{k_c}{k_1}\right)\left(\frac{k_c}{k_2} + \frac{k_{-2}}{k_2}\right) + \frac{k_c}{k_1}\right] + \frac{k_c}{k_{f1}}\left(1 + \frac{k_c}{k_2} + \frac{k_{-2}}{k_2}\right)\right\}[ES\text{–}Cu^{2+}] \quad (A.11)$$

Using (A.6), (A.8), (A.9), (A.10), and (A.11):

$$[ES\text{–}Cu^{2+}] = \frac{[E_{total}]}{\left(1 + \frac{k_c}{k_{f1}}\right)\left(1 + \frac{k_c}{k_2} + \frac{k_{-2}}{k_2}\right) + \left[\frac{k_c}{k_1} + \left(\frac{k_c}{k_1} + \frac{k_{-1}}{k_1}\right)\left(\frac{k_c}{k_2} + \frac{k_{-2}}{k_2}\right)\right]\left(1 + \frac{k_{b1}}{k_{f1}}\right) + \frac{k_{f2}}{k_{b2}}} \quad (A.12)$$

Here, $j_{cat,s}$ is ascribed to the catalytic reaction by ES and ES-Cu^{2+}, and is expressed as:

$$j_{cat,s} = n_{O_2}Fk_c([ES] + [ES\text{–}Cu^{2+}]) = \frac{j_{max}}{1 + \frac{k_c}{k_{f1}} + \frac{\left[\frac{k_c}{k_1} + \left(\frac{k_c}{k_1} + \frac{k_{-1}}{k_1}\right)\left(\frac{k_c}{k_2} + \frac{k_{-2}}{k_2}\right)\right]\left(1 + \frac{k_{b1}}{k_{f1}}\right) + \frac{k_{f2}}{k_{b2}}}{1 + \frac{k_c}{k_2} + \frac{k_{-2}}{k_2}}} \quad (A.13)$$

where the maximum catalytic current density (j_{max}) is defined as:

$$j_{max} = n_{O_2}Fk_c[E_{total}] \quad (A.14)$$

(A.13) can be simplified to:

$$j_{cat,s} = \frac{j_{max}}{1 + \frac{k_c}{k_{f1}} + \frac{\frac{k_{-1}}{k_1}\left[\frac{k_c}{k_{-1}}\frac{k_2}{k_{-2}} + \left(1 + \frac{k_c}{k_{-1}}\right)\left(1 + \frac{k_c}{k_{-2}}\right)\right]\left(1 + \frac{k_{b1}}{k_{f1}}\right) + \frac{k_2}{k_{-2}}\frac{k_{f2}}{k_{b2}}}{1 + \frac{k_c}{k_{-2}} + \frac{k_2}{k_{-2}}}} \quad (A.13')$$

Assuming that $\frac{k_c}{k_{-1}} \ll 1$ and $\frac{k_c}{k_{-2}} \ll 1$:

$$j_{\mathrm{cat,s}} = \frac{j_{\max}}{1 + \frac{k_{\mathrm{c}}}{k_{\mathrm{f1}}} + \frac{\frac{k_{-1}}{k_1}\left(1 + \frac{k_{\mathrm{b1}}}{k_{\mathrm{f1}}}\right) + \frac{k_2}{k_{-2}}\frac{k_{\mathrm{f2}}}{k_{\mathrm{b2}}}}{1 + \frac{k_2}{k_{-2}}}} \quad (\mathrm{A.13''})$$

Here, the kinetic constants can be expressed as:

$$\frac{k_{-1}}{k_1} = \frac{K_{\mathrm{O_2}}}{c_{\mathrm{O_2}}} \quad (\mathrm{A.15})$$

$$\frac{k_2}{k_{-2}} = \frac{c_{\mathrm{Cu^{2+}}}}{K_{\mathrm{Cu^{2+}}}} \quad (\mathrm{A.16})$$

$$k_{\mathrm{f}n} = {k^\circ}_n \eta_n^{-\alpha_n} \quad (n = 1,2) \quad (\mathrm{A.17})$$

$$k_{\mathrm{b}n} = {k^\circ}_n \eta_n^{1-\alpha_n} \quad (n = 1,2) \quad (\mathrm{A.18})$$

where α_n is the transfer coefficient (assumed to be 0.5) and η_n is defined as:

$$\eta_n = \exp\left\{\frac{F}{RT}(E - {E^{\circ\prime}}_n)\right\} \quad (\mathrm{A.19})$$

Using (A.15) to (A.19), (A.13′′) is re-expressed as:

$$j_{\mathrm{cat,s}} = \frac{j_{\max}}{1 + \frac{\eta_1^{0.5}}{\frac{{k^\circ}_1}{k_{\mathrm{c}}}} + \frac{\frac{K_{\mathrm{O_2}}}{c_{\mathrm{O_2}}}(1 + \eta_1) + \frac{c_{\mathrm{Cu^{2+}}}}{K_{\mathrm{Cu^{2+}}}}\eta_2^{-1}}{1 + \frac{c_{\mathrm{Cu^{2+}}}}{K_{\mathrm{Cu^{2+}}}}}} \quad (\mathrm{A.13'''})$$

Appendix B. Supplementary data

Supplementary data to this article can be found online at http://dx.doi.org/XXXXXXX.

References

[1] E.I. Solomon, U.M. Sundaram, T.E. Machonkin, Multicopper oxidases and oxygenases, Chem. Rev. 96 (1996) 2563–2605. https://doi.org/10.1021/cr950046o.

[2] T. Sakurai, K. Kataoka, Basic and applied features of multicopper oxidases, CueO, bilirubin oxidase, and laccase, Chem. Rec. 7 (2007) 220–229. https://doi.org/10.1002/tcr.20125.

[3] N. Mano, A. de Poulpiquet, O_2 reduction in enzymatic biofuel cells, Chem. Rev. 118 (2018) 2392–2468. https://doi.org/10.1021/acs.chemrev.7b00220.

[4] M. Miyata, Y. Kitazumi, O. Shirai, K. Kataoka, K. Kano, Diffusion limited biosensing of dissolved oxygen by direct electron transfer-type bioelectrocatalysis of multi-copper oxidases immobilized on porous gold microelectrodes. J. Electroanal. Chem. 860 (2020) 113895. https://doi.org/10.1016/j.jelechem.2020.113895.

[5] R.D. Milton, S.D. Minteer, Direct enzymatic bioelectrocatalysis: differentiating between myth and reality, J. R. Soc. Interface 14 (2017) 20170253. https://doi.org/10.1098/rsif.2017.0253.

[6] N.D.J. Yates, M.A. Fascione, A. Parkin, Methodologies for “wiring” redox proteins/enzymes to electrode surfaces, Chem. Eur. J. 24 (2018) 12164–12182. https://doi.org/10.1002/chem.201800750.

[7] M. Sensi, M. del Barrio, C. Baffert, V. Fourmond, C. Léger, New perspectives in hydrogenase direct electrochemistry, Curr. Opin. Electrochem. 5 (2017) 135–145. https://doi.org/10.1016/j.coelec.2017.08.005.

[8] F.A. Armstrong, Some fundamental insights into biological redox catalysis from

the electrochemical characteristics of enzymes attached directly to electrodes, Electrochim. Acta 390 (2021) 138836. https://doi.org/10.1016/j.electacta.2021.138836.

[9] P. Bollella, L. Gorton, R. Antiochia, Direct electron transfer of dehydrogenases for development of 3rd generation biosensors and enzymatic fuel cells, Sensors 18 (2018) 1319. https://doi.org/10.3390/s18051319.

[10] L. Pilan, Tailoring the performance of electrochemical biosensors based on carbon nanomaterials via aryldiazonium electrografting, Bioelectrochemistry 138 (2021) 107697. https://doi.org/10.1016/j.bioelechem.2020.107697.

[11] N. Lalaoui, M. Holzinger, A. Le Goff, S. Cosnier, Diazonium functionalisation of carbon nanotubes for specific orientation of multicopper oxidases: Controlling electron entry points and oxygen diffusion to the enzyme, Chem. Eur. J. 22 (2016) 10494–10500. https://doi.org/10.1002/chem.201601377.

[12] K. Stolarczyk, D. Łyp, K. Zelechowska, J.F. Biernat, J. Rogalski, R. Bilewicz, Arylated carbon nanotubes for biobatteries and biofuel cells, Electrochim. Acta 79 (2012) 74–81. https://doi.org/10.1016/j.electacta.2012.06.050.

[13] F. Tasca, W. Harreither, R. Ludwig, J.J. Gooding, L. Gorton, Cellobiose dehydrogenase aryl diazonium modified single walled carbon nanotubes: enhanced direct electron transfer through a positively charged surface, Anal. Chem. 83 (2011) 3042–3049. https://doi.org/10.1021/ac103250b.

[14] A. Hyre, K. Casanova-Hampton, S. Subashchandrabose, Copper homeostatic mechanisms and their role in the virulence of *Escherichia coli* and *Salmonella enterica*, EcoSal Plus, 9 (2020) 0014. https://doi.org/10.1128/ecosalplus.ESP-0014-2020.

[15] A. Andrei, Y. Öztürk, B. Khalfaoui-Hassani, J. Rauch, D. Marckmann, P.-I. Trasnea, F. Daldal, H.-G. Koch, Cu homeostasis in bacteria: the ins and outs, Membranes 10 (2020) 242. https://doi.org/10.3390/membranes10090242.

[16] S.K. Singh, S.A. Roberts, S.F. McDevitt, A. Weichsel, G.F. Wildner, G.B. Grass, C. Rensing, W.R. Montfort, Crystal structures of multicopper oxidase CueO bound to copper(I) and silver(I): functional role of a methionine-rich sequence, J. Biol. Chem. 286 (2011) 37849–37857. https://doi.org/10.1074/jbc.M111.293589.

[17] I. Mazurenko, T. Adachi, B. Ezraty, M. Ilbert, K. Sowa, E. Lojou, Electrochemistry of copper efflux oxidase-like multicopper oxidases involved in copper homeostasis, Curr. Opin. Electrochem. 32 (2022) 100919. https://doi.org/10.1016/j.coelec.2021.100919.

[18] K. Kataoka, H. Komori, Y. Ueki, Y. Konno, Y. Kamitaka, S. Kurose, S. Tsujimura, Y. Higuchi, K. Kano, D. Seo, T. Sakurai, Structure and function of the engineered multicopper oxidase CueO from *Escherichia coli*–Deletion of the methionine-rich helical region covering the substrate-binding site, J. Mol. Biol. 373 (2007) 141–152. https://doi.org/10.1016/j.jmb.2007.07.041.

[19] S. Kurose, K. Kataoka, K. Otsuka, Y. Tsujino, T. Sakurai, Promotion of laccase activities of *Escherichia coli* cuprous oxidase, CueO by deleting the segment covering the substrate binding site, Chem. Lett. 36 (2007) 232–233. https://doi.org/10.1246/cl.2007.232.

[20] S.A. Roberts, G.F. Wildner, G. Grass, A. Weichsel, A. Ambrus, C. Rensing, W.R. Montfort, A labile regulatory copper ion lies near the T1 copper site in the multicopper oxidase CueO, J. Biol. Chem. 278 (2003) 31958–31963. https://doi.org/10.1074/jbc.M302963200.

[21] T. Adachi, Y. Kitazumi, O. Shirai, T. Kawano, K. Kataoka, K. Kano, Effects of elimination of α helix regions on direct electron transfer-type bioelectrocatalytic properties of copper efflux oxidase, Electrochemistry 88 (2020) 185–189. https://doi.org/10.5796/electrochemistry.20-00015.

[22] V.P. Hitaishi, R. Clément, L. Quattrocchi, P. Parent, D. Duché, L. Zuily, M. Ilbert, E. Lojou, I. Mazurenko, Interplay between orientation at electrodes and copper activation of *Thermus thermophilus* laccase for O_2 reduction, J. Am. Chem. Soc. 142 (2020) 1394–1405. https://doi.org/10.1021/jacs.9b11147.

[23] M. Valles, A.F. Kamaruddin, L.S. Wong, C.F. Blanford, Inhibition in multicopper oxidases: a critical review, Catal. Sci. Technol. 10 (2020) 5386–5410. https://doi.org/10.1039/D0CY00724B.

[24] R. Antiochia, D. Oyarzun, J. Sánchez, F. Tasca, Comparison of direct and mediated electron transfer for bilirubin oxidase from Myrothecium verrucaria. Effects of inhibitors and temperature on the oxygen reduction reaction, Catalysts 9 (2019) 1056. https://doi.org/10.3390/catal9121056.

[25] A. de Poulpiquet, C.H. Kjaergaard, J. Rouhana, I. Mazurenko, P. Infossi, S. Gounel, R. Gadiou, M.T. Giudici-Orticoni, E.I. Solomon, N. Mano, E. Lojou, Mechanism of chloride inhibition of bilirubin oxidases and its dependence on potential and pH, ACS Catal. 7 (2017) 3916–3923. https://doi.org/10.1021/acscatal.7b01286.

[26] F. Tasca, D. Farias, C. Castro, C. Acuna-Rougier, R. Antiochia, Bilirubin oxidase from Myrothecium verrucaria physically absorbed on graphite electrodes. Insights into the alternative resting form and the sources of activity loss, PLoS ONE 10 (2015) e0132181. https://doi.org/10.1371/journal.pone.0132181.

[27] C.H. Kjaergaard, F. Durand, F. Tasca, M.F. Qayyum, B. Kauffmann, S. Gounel, E. Suraniti, K.O. Hodgson, B. Hedman, N. Mano, E.I. Solomon, Spectroscopic and crystallographic characterization of “alternative resting” and “resting oxidized” enzyme forms of bilirubin oxidase: Implications for activity and electrochemical behavior of multicopper oxidases, J. Am. Chem. Soc. 134 (2012) 5548–5551. https://doi.org/10.1021/ja211872j.

[28] J. Hirose, K. Inoue, H. Sakuragi, M. Kikkawa, M. Minakami, T. Morikawa, H. Iwamoto, K. Hiromi, Anions binding to bilirubin oxidase from *Trachyderma tsunodae* K-2593, Inorganica Chim. Acta 273 (1998) 204–212. https://doi.org/10.1016/S0020-1693(97)06183-5.

[29] S. Gounel, J. Rouhana, C. Stines-Chaumeil, M. Cadet, N. Mano, Increasing the catalytic activity of Bilirubin oxidase from *Bacillus pumilus*: Importance of host strain and chaperones proteins, J. Biotechnol. 230 (2016) 19–25. https://doi.org/10.1016/j.jbiotec.2016.04.035.

[30] K.A. Vincent, A. Parkin, F.A. Armstrong, Investigating and exploiting the electrocatalytic properties of hydrogenases, Chem. Rev. 107 (2007) 4366–4413. https://doi.org/10.1021/cr050191u.

[31] K. So, R. Hamamoto, R. Takeuchi, Y. Kitazumi, O. Shirai, R. Endo, H. Nishihara, Y. Higuchi, K. Kano, Bioelectrochemical analysis of thermodynamics of the catalytic cycle and kinetics of the oxidative inactivation of oxygen-tolerant [NiFe]-hydrogenase, J. Electroanal. Chem. 766 (2016) 152–161. https://doi.org/10.1016/j.jelechem.2016.02.009.

[32] V. Ducros, A.M. Brzozowski, K.S. Wilson, S.H. Brown, P. Østergaard, P. Schneider, D.S. Yaver, A.H. Pedersen, G.J. Davies, Crystal structure of the type-2

Cu depleted laccase from *Coprinus cinereus* at 2.2 Å resolution, Nat. Struct. Biol. 5 (1998) 310–316. https://doi.org/10.1038/nsb0498-310.

[33] N. Hakulinen, L.-L. Kiiskinen, K. Kruus, M. Saloheimo, A. Paananen, A. Koivula, J. Rouvinen, Crystal structure of a laccase from *Melanocarpus albomyces* with an intact trinuclear copper site, Nat. Struct. Biol. 9 (2002) 601–605. https://doi.org/10.1038/nsb823.

[34] K. Piontek, M. Antorini, T. Choinowski, Crystal structure of a laccase from the fungus *Trametes versicolor* at 1.90-Å resolution containing a full complement of coppers, J. Biol. Chem. 277 (2002) 37663–37669. https://doi.org/10.1074/jbc.M204571200.

[35] X. Li, Z. Wei, M. Zhang, X. Peng, G. Yu, M. Teng, W. Gong, Crystal structures of *E. coli* laccase CueO at different copper concentrations, Biochem. Biophys. Res. Commun. 354 (2007) 21–26. https://doi.org/10.1016/j.bbrc.2006.12.116.

[36] A.J. Bard, R. Parsons, J. Jordan, Standard potential in aqueous solution, Marcel Dekker (1985). https://doi.org/10.1201/9780203738764.

[37] F. Xu, W. Shin, S.H. Brown, J.A. Wahleithner, U.M. Sundaram, E.I. Solomon, A study of a series of recombinant fungal laccases and bilirubin oxidase that exhibit significant differences in redox potential, substrate specificity, and stability, Biochem. Biphys. Acta 1292 (1996) 303–311. https://doi.org/10.1016/0167-4838(95)00210-3.

[38] R. Clément, X. Wang, F. Biaso, M. Ilbert, I. Mazurenko, E. Lojou, Mutations in the coordination spheres of T1 Cu affect Cu^{2+}-activation of the laccase from *Thermus thermophilus*, Biochimie 182 (2021) 228–237. https://doi.org/10.1016/j.biochi.2021.01.006.

[39] A.A. Hamdan, P.-P. Liebgott, V. Fourmond, O. Gutiérrez-Sanz, A.L. De Lacey, P. Infossi, M. Rousset, S. Dementin, C. Léger, Relation between anaerobic inactivation and oxygen tolerance in a large series of NiFe hydrogenase mutants, Proc. Natl. Acad. Sci. USA 109 (2012) 19916–19921. https://doi.org/10.1073/pnas.1212258109.

[40] D.M. Himmelblau, Diffusion of dissolved gases in liquids. Chem. Rev. 64 (1964) 527–550. https://doi.org/10.1021/cr60231a002.

[41] A. Nagashima, Viscosity of water substance–new international formulation and its background, J. Phys. Chem. Ref. Data 6 (1977) 1133–1166. https://doi.org/10.1063/1.555562.

[42] IUPAC Solubility Data Series (Ed. R. Battino), "Oxygen and Ozone", Vol. 7, Pergamon Press, Oxford (1981).

[43] P.J. Butterworth, The use of dixon plots to study enzyme inhibition, Biochim. Biophys. Acta 289 (1972) 251–253. https://doi.org/10.1016/0005-2744(72)90074-5.

[44] G.A. Grant, The many faces of partial inhibition: Revealing imposters with graphical analysis, Arch. Biochem. Biophys. 653 (2018) 10–23. https://doi.org/10.1016/j.abb.2018.06.009.

[45] K. Kataoka, T. Sakurai, Role of hydrogen bond connecting ligands for substrate and type I copper in copper(I) oxidase CueO, Chem. Lett. 42 (2013) 1102–1104. https://doi.org/10.1246/cl.130422.

[46] E.I. Solomon, A.J. Augustine, J. Yoon, O_2 reduction to H_2O by the multicopper oxidases, Dalton Trans. 30 (2008) 3921–3932. https://doi.org/10.1039/B800799C.

[47] H. Komori, R. Sugiyama, K. Kataoka, Y. Higuchi, T. Sakurai, An O-centered

structure of the trinuclear copper center in the Cys500Ser/Glu506Gln mutant of CueO and structural changes in low to high X-ray dose conditions, Angew. Chem. Int. Ed. 51 (2012) 1–5. https://doi.org/10.1002/anie.201107739.

[48] H. Wang, X. Liu, J. Zhao, Q. Yue, Y. Yan, Z. Gao, Y. Dong, Z. Zhang, Y. Fan, J. Tian, N. Wu, Y. Gong, Crystal structures of multicopper oxidase CueO G304K mutant: structural basis of the increased laccase activity, Sci. Rep. 8 (2018) 14252. https://doi.org/10.1038/s41598-018-32446-7.

Figure captions

Figure 1. (A) CVs for O_2 reduction at (A) rCueO- and (B) ΔαCueO-modified CNT-NH_2/GCs in 0.1 M acetate buffer (pH 5.0) at 25 °C in an O_2-saturated atmosphere at a scan rate (υ) of 5 mV s^{-1} and ω = 4000 rpm (broken lines). The solid lines correspond to CVs recorded in the presence of $CuSO_4$ at the concentration indicated at the left of each curve. The dotted red lines correspond to CVs recorded in a N_2-saturated atmosphere in the absence of $CuSO_4$. The insets show enlarged voltammograms.

Figure 2. CVs at various scan rates recorded at the rCueO-modified CNT-NH_2/GC in 0.1 M acetate buffer (pH 5.0) containing 0.5 mM $CuSO_4$ at 25 °C in an O_2-saturated atmosphere at ω = 4000 rpm. The scan rate is indicated at left of each curve. The broken line corresponds to the CV recorded in the absence of $CuSO_4$ at υ = 5 mV s^{-1}.

Figure 3. Multi-scanned CVs at the rCueO-modified CNT-NH_2/GC in 0.1 M acetate buffer (pH 5.0) containing 1 mM $CuSO_4$ at 25 °C in an O_2-saturated atmosphere at υ = 10 mV s^{-1} and ω = 4000 rpm (solid lines), swept to the lowest potentials of (A) 0.3 V and (B) 0.2 V. The broken lines correspond to CVs recorded in the absence of $CuSO_4$. The dotted lines correspond to CVs recorded at the CNT-NH_2/GC without enzyme modifications in the presence of 1 mM $CuSO_4$. The insets show enlarged voltammograms.

Figure 4. CAs at (A) rCueO- and (B) ΔαCueO-modified CNT-NH_2/GCs in 0.1 M acetate buffer (pH 5.0) at 25 °C in an O_2-saturated atmosphere at ω = 4000 rpm and E = 0.35 V, in the presence of $CuSO_4$ at concentrations indicated at the right of each curve. The open circles and dotted lines correspond to experimental and refined values, respectively.

Figure 5. Refined k_I and k_A values for rCueO (circles) and ΔαCueO (squares). (A, B) Relationships between the potential and the common logarithms of k_I and k_A in the presence of 1 mM $CuSO_4$, respectively. (C, D) Relationships between k_I and k_A, and the $CuSO_4$ concentration at 0.35 V, respectively. Error bars were evaluated using Student's *t*-distributions at a 90% confidence level (n = 5).

Figure 6. Lineweaver–Burk and Dixon plots for (A, B) rCueO and (C, D) ΔαCueO at E = 0.35 V. Error bars were evaluated using Student's *t*-distributions at a 90% confidence level (n = 5). The dotted lines indicate regression lines.

Figure 7. Linear sweep voltammograms for O_2 reduction at rCueO- (circles) and ΔαCueO- (squares) modified CNT-NH_2/GCs in 0.1 M acetate buffer (pH 5.0) at 25 °C in an O_2-saturated atmosphere at ω = 4000 rpm, in the absence of Cu^{2+}. The dotted lines correspond to refined curves determined by non-linear regression analysis based on Eq. (8).

Figure 8. Steady-state current densities for Cu^{2+}-dependent reductive inactivation at (A) rCueO- and (B) ΔαCueO-modified CNT-NH_2/GCs in 0.1 M acetate buffer (pH 5.0) at 25 °C in an O_2-saturated atmosphere at ω = 4000 rpm. Errors were evaluated using Student's *t*-distributions at a 90% confidence level (n = 5). The dotted lines correspond to refined curves determined by non-linear regression analysis based on Eq. (9).

Figure 9. Crystal structures of rCueO (A; PDB: 3OD3) and ΔαCueO (B; PDB: 2YXV).

Scheme 1. Proposed model for the Cu^{2+}-dependent reductive inactivation of CueO.

Notations:

E_R: the reduced state of the enzyme

E_O: the oxidized state of the enzyme

ES: the enzyme-substrate complex

ES-Cu^{2+}: the active state of the enzyme-substrate-inhibitor complex

ES-Cu^{+}: the inactive state of the enzyme-substrate-inhibitor complex

k_c: the catalytic constant

k_1: the kinetic constant of coordination between the enzyme and the substrate

k_{-1}: the kinetic constant of dissociation between the enzyme and the substrate

k_{f1}: the forward electrode kinetic constant of the electrode-active site of the enzyme

k_{b1}: the backward electrode kinetic constant of the electrode-active site of the enzyme

k_2: the kinetic constant of coordination between the enzyme and the inhibitor

k_{-2}: the kinetic constant of dissociation between the enzyme and the inhibitor

k_{f2}: the forward electrode kinetic constant of the inhibitor-binding site of the enzyme

k_{b2}: the backward electrode kinetic constant of the inhibitor-binding site of the enzyme

Scheme 2. Proposed mechanism for the Cu^{2+}-dependent reductive inactivation of CueO.

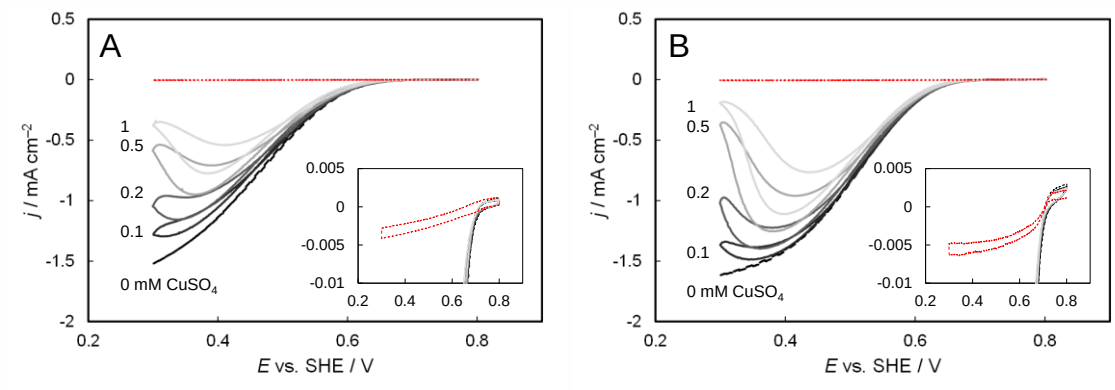

Figure 1.

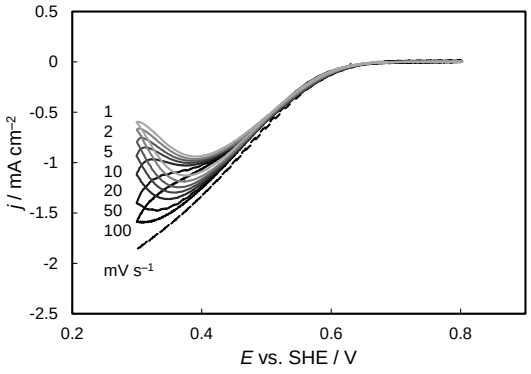

Figure 2.

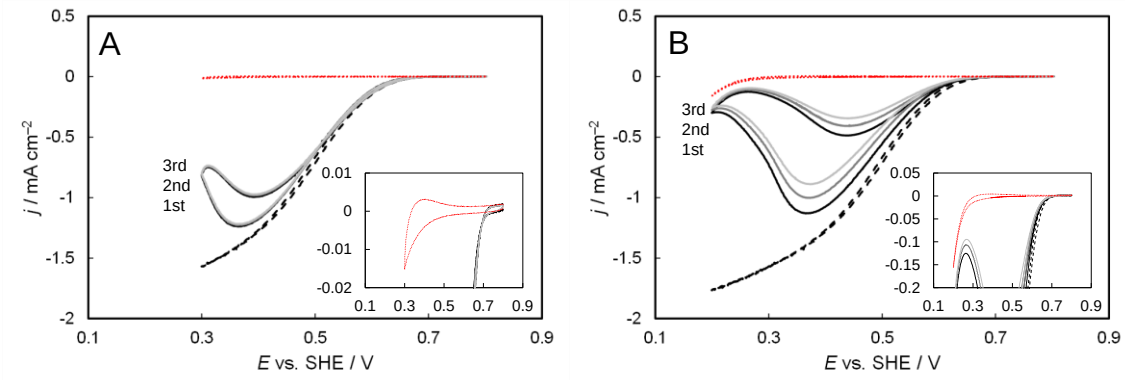

Figure 3.

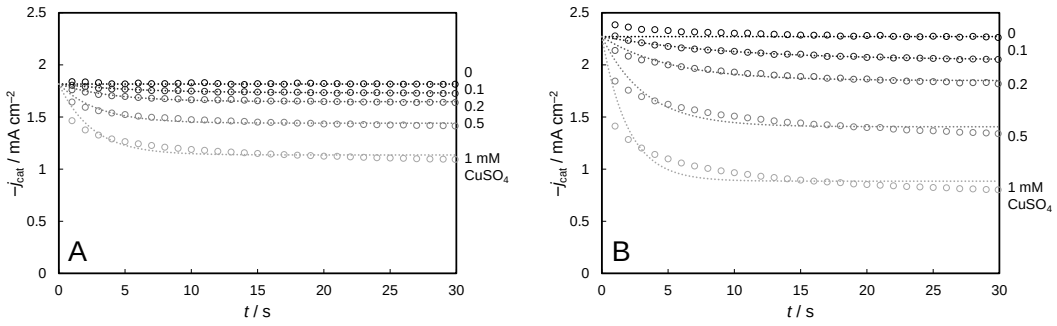

Figure 4.

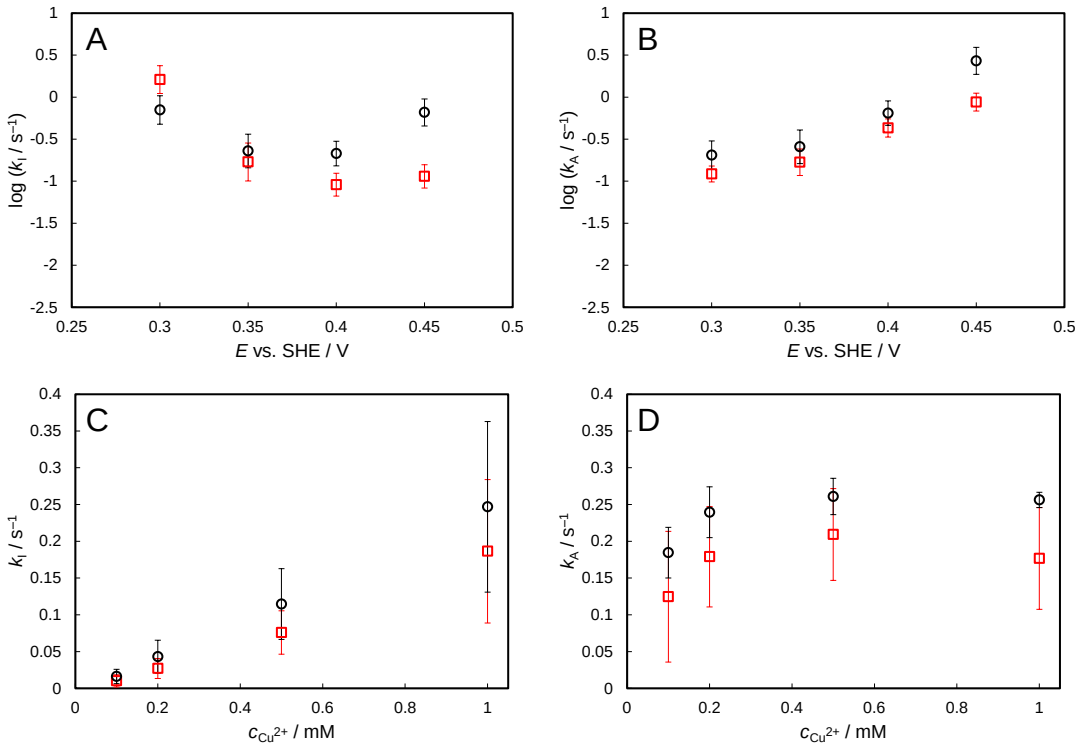

Figure 5.

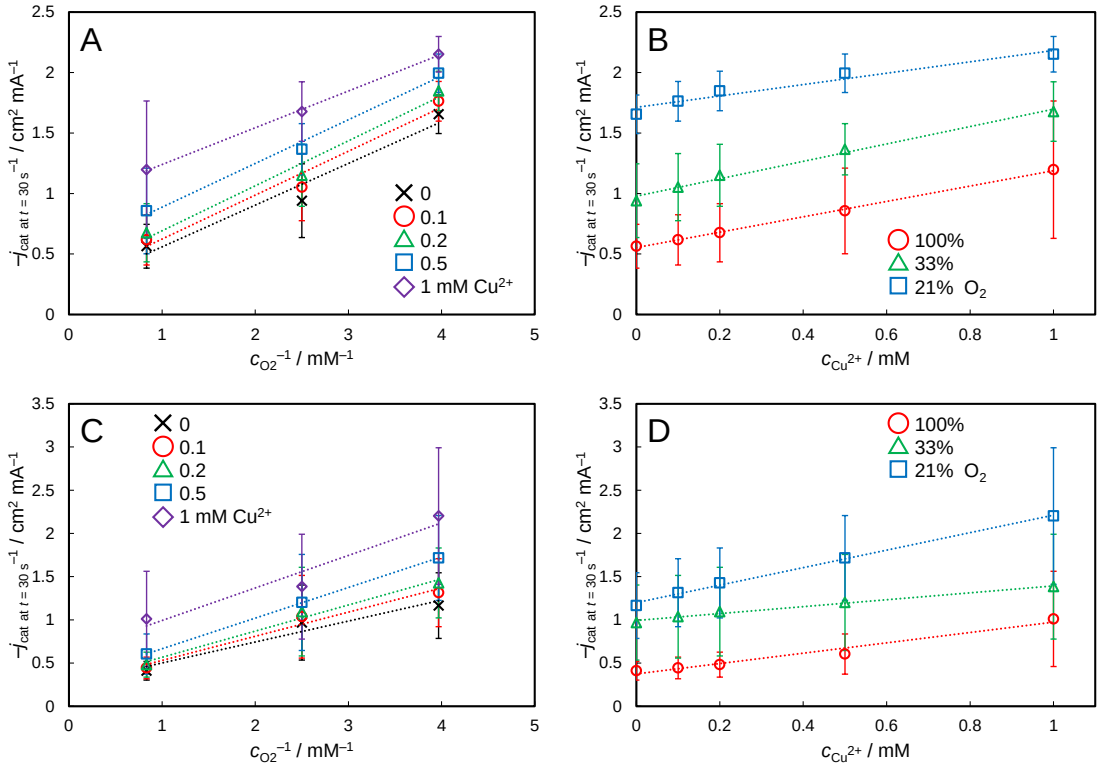

Figure 6.

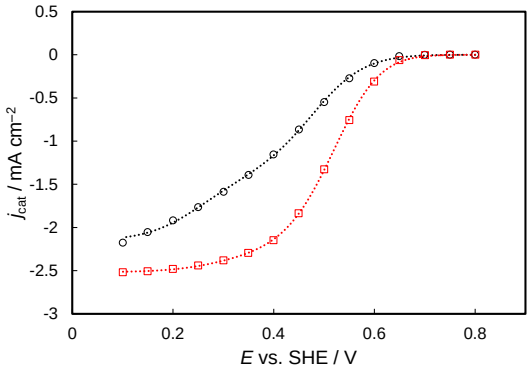

Figure 7.

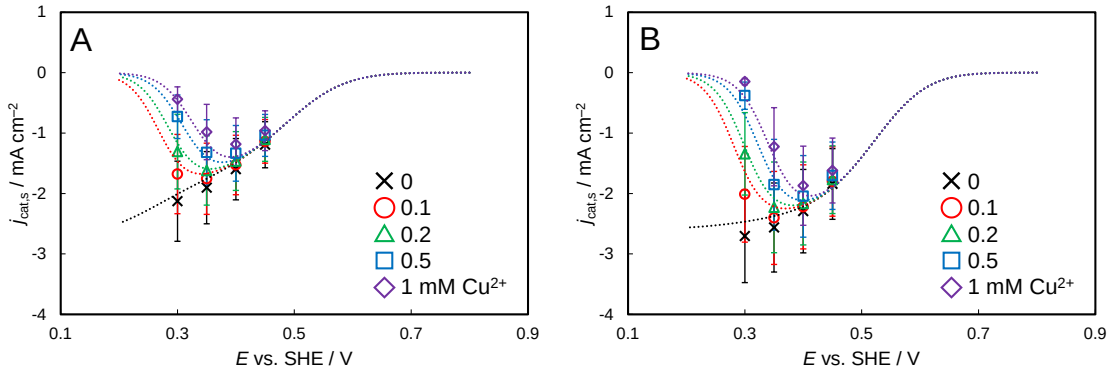

Figure 8.

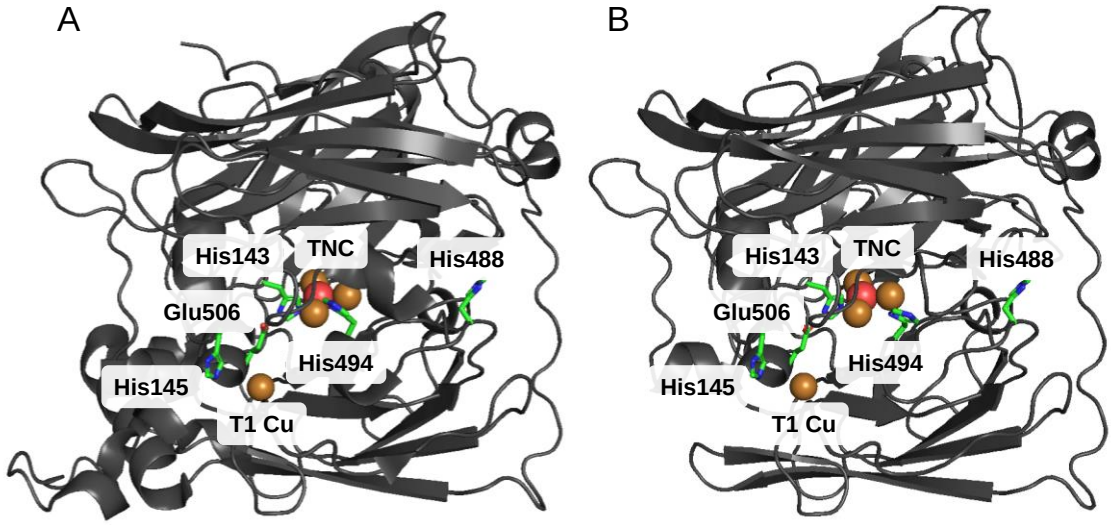

Figure 9.

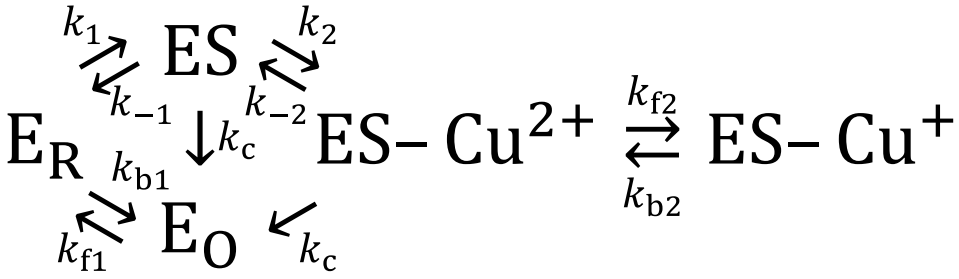

Scheme 1.

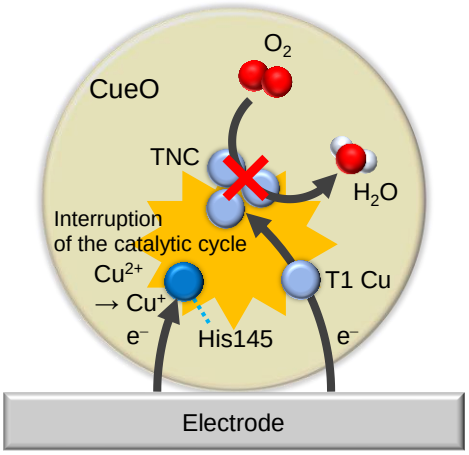

Scheme 2.

Table 1. Refined data obtained by the non-linear regression analyses of voltammograms. Errors were evaluated from Student's *t*-distribution at a 90% confidence level (n = 5).

	$E^{\circ\prime}_1$ / V	k°_{max} / k_c	$-j_{max}$ / mA cm^{-2}	p_1	p_2	p_3
rCueO	0.465 ± 0.007	1.6 ± 0.7	2.3 ± 0.3	0.6 ± 0.1	0.10 ± 0.05	0.3 ± 0.1
ΔαCueO	0.464 ± 0.003	3.0 ± 0.6	2.6 ± 0.4	0.91 ± 0.03	0.03 ± 0.03	0.06 ± 0.03

Table 2. Refined data obtained by the non-linear regression analyses of j_{cat} values at t = 30 s. Errors were evaluated from Student's *t*-distribution at a 90% confidence level (n = 5).

	$-j_{max}$ / mA cm^{-2}	$K_{Cu^{2+}}\exp\left(-\frac{F}{RT}E^{\circ\prime}_2\right)$ / mM
rCueO	2.8 ± 0.9	(1.9 ± 0.7) × 10^{-6}
ΔαCueO	2.6 ± 0.8	(1.6 ± 0.7) × 10^{-6}